nature nanotechnology

Article

https://doi.org/10.1038/s41565-023-01550-9

Nanoscale one-dimensional close packing of interfacial alkali ions driven by water-mediated attraction

Received: 30 August 2022

Accepted: 17 October 2023

Published online: 04 December 2023

Check for updates

Ye Tian[1,9], Yizhi Song[1,9], Yijie Xia[2,9], Jiani Hong[1,9], Yupeng Huang[2], Runze Ma[1], Sifan You[1], Dong Guan[1], Duanyun Cao[1], Mengze Zhao[3], Ji Chen[4,5], Chen Song[6], Kaihui Liu[3,5,7], Li-Mei Xu[1,5,7] ✉, Yi Qin Gao[2] ✉, En-Ge Wang[1,5,7,8] ✉ & Ying Jiang[1,5,7] ✉

The permeability and selectivity of biological and artificial ion channels correlate with the specific hydration structure of single ions. However, fundamental understanding of the effect of ion–ion interaction remains elusive. Here, via non-contact atomic force microscopy measurements, we demonstrate that hydrated alkali metal cations (Na^+ and K^+) at charged surfaces could come into close contact with each other through partial dehydration and water rearrangement processes, forming one-dimensional chain structures. We prove that the interplay at the nanoscale between the water–ion and water–water interaction can lead to an effective ion–ion attraction overcoming the ionic Coulomb repulsion. The tendency for different ions to become closely packed follows the sequence $K^+ > Na^+ > Li^+$, which is attributed to their different dehydration energies and charge densities. This work highlights the key role of water molecules in prompting close packing and concerted movement of ions at charged surfaces, which may provide new insights into the mechanism of ion transport under atomic confinement.

The atomic-scale arrangement and transport of hydrated ions under confined geometry play crucial roles in water desalination[1–6], aqueous and non-aqueous secondary batteries[7–10], biological ion channels[11,12] and other applied fields or natural phenomena. Ion hydration and dehydration processes are critical for the permeability and selectivity of both biological and artificial ion channels[12–14]. So far, the understanding is based on the ion-specific hydration structure of individual ions, with little knowledge of ion–ion interaction[15,16]. Under strongly confined geometries (subnanometre), especially those with charged channel walls, the local ion concentration is usually high (~several tens of molar), such that the effect of ion–ion interaction becomes important and plays a decisive role in the channel's functioning[17–19]. It is speculated

[1]International Center for Quantum Materials, School of Physics, Peking University, Beijing, People's Republic of China. [2]Institute of Theoretical and Computational Chemistry, College of Chemistry and Molecular Engineering, Peking University, Beijing, People's Republic of China. [3]State Key Laboratory for Mesoscopic Physics, Frontiers Science Centre for Nano-optoelectronics, School of Physics, Peking University, Beijing, China. [4]School of Physics, Peking University, Beijing, People's Republic of China. [5]Interdisciplinary Institute of Light-Element Quantum Materials and Research Center for Light-Element Advanced Materials, Peking University, Beijing, People's Republic of China. [6]Center for Quantitative Biology, Academy for Advanced Interdisciplinary Studies, Peking University, Beijing, People's Republic of China. [7]Collaborative Innovation Center of Quantum Matter, Beijing, People's Republic of China. [8]Songshan Lake Materials Laboratory, Institute of Physics, CAS and School of Physics, Liaoning University, Shenyang, People's Republic of China. [9]These authors contributed equally: Ye Tian, Yizhi Song, Yijie Xia, Jiani Hong. ✉e-mail: limei.xu@pku.edu.cn; gaoyq@pku.edu.cn; egwang@pku.edu.cn; yjiang@pku.edu.cn

https://doi.org/10.1038/s41565-023-01550-9

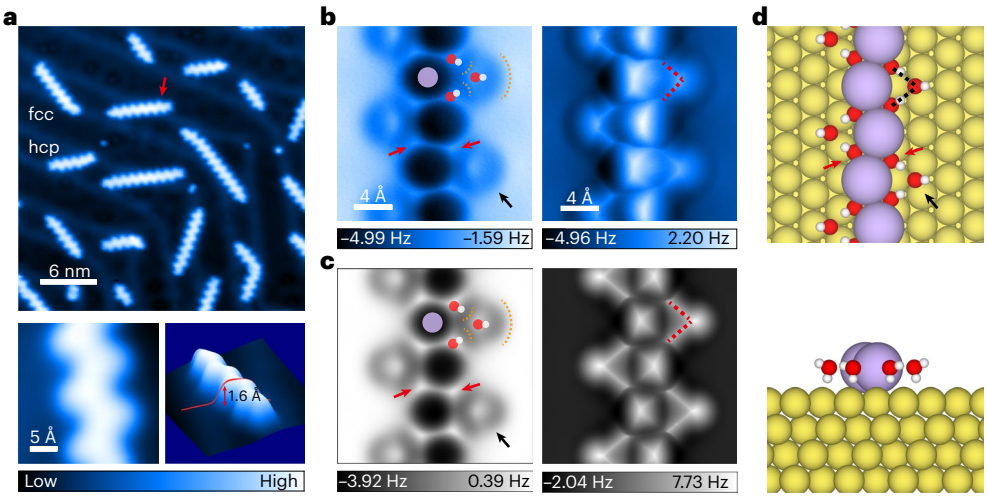

Fig. 1 | Atomic structure of the 1D K^+–water chain. a, Constant-current STM images of the 1D K^+–water chains on Au(111). Upper: the K^+–water chains adsorbed in hcp regions with three orientations, [$\bar{1}$01], [01$\bar{1}$], [0$\bar{1}$1]. The longer chains can extend over the herringbone structure (indicated by a red arrow). hcp, hexagonal close packing; fcc, face-centred cubic. Lower left: a zoomed-in STM image of a K^+–water zigzag chain. Lower right: a line profile across the edge showing the height of the chain (~1.6 Å). Set point of the STM images: 100 mV, 10 pA. **b**, Constant-height AFM (frequency shift, Δf) images at the tip heights of 0 pm (left) and −100 pm (right). **c**, Simulated AFM images at the tip heights of 11.40 Å (left) and 10.75 Å (right). **d**, Top and side views of a structural model of the K^+–water chain on the Au(111) surface. Au, K, H and O atoms are denoted by yellow, purple, white and red spheres, respectively. The orange dashed curves in **b** and **c** highlight the crooked depressions, arising from the H of the water molecules. The bridging water molecules and adjacent bridging water molecules are indicated by red and black arrows, respectively, in **b**–**d**. The black (red) dashed lines in **d** (**b** and **c**) indicate the H bonds in the structural model (AFM images). The tip heights in **b** are referenced to the STM set point on the Au substrate (100 mV, 10 pA). The tip heights in **c** are defined as the vertical distance between the apex atom of the metal tip and the outermost atom of the Au substrate. The oscillation amplitude of experimental and simulated images is 100 pm. All the experiments were performed at 5 K.

from theoretical calculations that the dehydration of alkali metal ions under atomic-scale confinement may lead to close ion–ion contact, which contributes to the high permeation rate and selectivity of ion channels (the diffusion rate of K^+ in the K^+ channel is ~10^8 ions s^{-1}, which is 1,000 times larger than that of Na^+) through the direct Coulomb knock-on and concerted ion movement[18,20]. Although spectroscopic investigations have evidenced high-density ionic accumulation (charge density of ~1.8×10^{14} cm^{-2}) under two-dimensional (2D) confinement and in superconcentrated aqueous solutions (~27 M), the detailed configuration of ionic close packing has not been observed via experimental measurements[17,21]. Moreover, considering the strong electrostatic repulsion between the ions, the driving force for the close packing of hydrated ions is still unclear.

In this work, we fabricated samples with continuously tunable ratios of alkali metal cations (Li^+, Na^+ and K^+) and water molecules (Methods and Supplementary Figs. 1 and 2). The alkali metal cations could assemble into one-dimensional (1D) chain structures together with water molecules on charged metal (Au(111)) and monolayer graphene surfaces. A qPlus-based atomic force microscope (AFM)[22] (Methods) was used to image the 1D chain structures with atomic resolution, revealing that the ions (Na^+ or K^+) are in close contact with each other. The tip manipulation experiment and theoretical simulation indicate that the close packing of alkali cations involves partial dehydration and the formation of new water hydrogen (H) bonds. These 1D ion chains show water-mediated ionic attraction, ion-specific hydration structure and collective movement, which may shed new light on the permeation ability and selectivity of ion channels.

Single 1D K^+–water chains

Figure 1a shows scanning tunnelling microscope (STM) images of 1D K^+–water chain structures on single-crystal Au(111), formed by co-depositing K atoms and water molecules (Methods). As the K atom lands on the Au(111) surface, it is ionized to a K^+ cation by transferring electrons to the Au substrate and water molecules, leading to electrostatic and dispersion interactions between the K^+ and the Au substrate (Supplementary Section 1, Supplementary Figs. 3 and 4). These K^+–water 1D chains exhibit three equivalent directions ([$\bar{1}$01], [01$\bar{1}$], [0$\bar{1}$1]) and are mainly located within the hexagonal close packing (hcp) regions of the Au(111) surface (Fig. 1a, upper panel). Some chains can extend across the herringbone reconstructions into the face-centred cubic regions (indicated by a red arrow in Fig. 1a). Short chains, consisting of a minimum number of three K^+ ions (Supplementary Section 2 and Supplementary Fig. 5), can diffuse on the surface through either tip manipulation or thermal excitation (Supplementary Fig. 6 and Supplementary Video 1), indicating the stability of the K^+–water chains and the concerted ion movement. The line profile across the 1D chain suggests a single-layer height (Fig. 1a, lower right panel). Even though the STM can reach a molecular resolution of water at metal interfaces[23], the zoomed-in STM image shows a zigzag structure without internal resolution for the K^+–water chain (Fig. 1a, lower left panel).

In contrast, the AFM images reveal more details of the K^+–water chain (Fig. 1b,c). At a large tip height (Fig. 1b, left), a round depression results from the attractive force between the positively charged K^+ and the negatively charged carbon monoxide (CO)-terminated tip[24–26]. The multipole electrostatic force between the CO tip and the water molecule allows us to distinguish the negatively charged O (protrusion) and positively charged H (depression, indicated by orange dashed curves)[27], indicating the H-down configuration of water molecules because of the negatively charged Au substrate (Supplementary Section 1 and Supplementary Fig. 3). At a small tip height (Fig. 1b, right), the Pauli repulsion force dominates the image contrast, and prominent sharp lines appear (dashed lines), resembling the H bonds between the water molecules[28,29].

On the basis of the high-resolution AFM images obtained at systematically varied tip heights (Supplementary Fig. 7), we propose an atomic model for the 1D K^+–water chain with a water–ion ratio of 3:1 (Fig. 1d), the stability of which is confirmed by ab initio density

https://doi.org/10.1038/s41565-023-01550-9

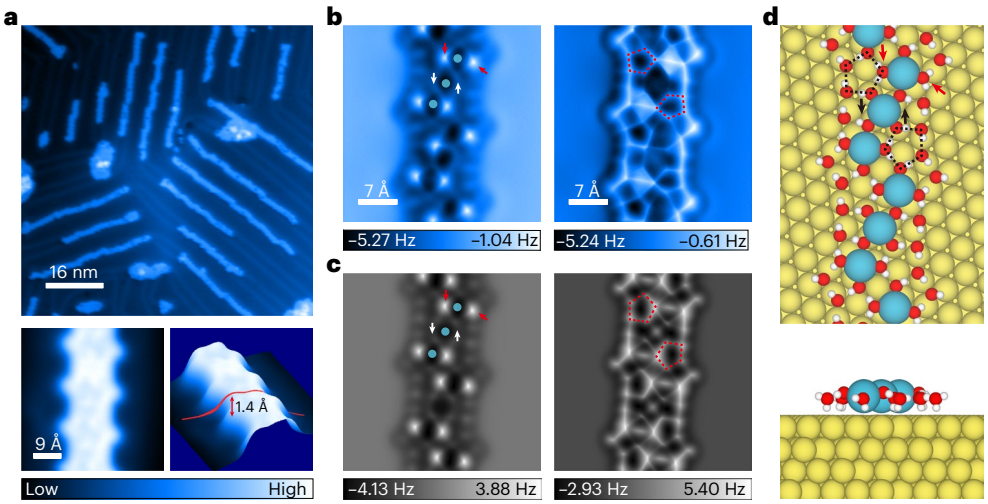

Fig. 2 | Atomic structure of the 1D Na^+–water chain. a, Constant-current STM images of the 1D Na^+–water chains on Au(111). Upper: the Na^+–water chains adsorbed in hcp regions along the herringbone structure. Lower left: a zoomed-in STM image of a Na^+–water chain. Lower right: a line profile across the edge showing the height of the chain (~1.4 Å). Set point of the STM images: 100 mV, 10 pA. **b**, Constant-height AFM (Δf) images at the tip heights of 38 pm (left) and −20 pm (right). **c**, Simulated AFM images at the tip heights of 11.54 Å (left) and 11.14 Å (right). **d**, The structural model of the Na^+–water chain structure on the Au(111) surface. Au, Na, H and O atoms are denoted by yellow, cyan, white and red spheres, respectively. The bridging water molecules are indicated by black (white) arrows in **d** (**b** and **c**). The flat-lying water molecules are indicated by red arrows in **b**–**d**. The water pentagons are indicated by black (red) dashed lines in **d** (**b** and **c**). All the tip heights in **b** and **c** have the same reference and definition as shown in Fig. 1. The oscillation amplitude of experimental and simulated images is 100 pm. All the experiments were performed at 5 K.

functional theory (DFT) calculations (Methods). Noteworthily, the K^+ ions are in close contact with each other and bridged by two water molecules (indicated by red arrows in Fig. 1b–d). The water molecule at the chain edge accepts two H bonds from the adjacent bridging water molecules (indicated by black arrows in Fig. 1b–d). The simulated AFM images (Fig. 1c and Supplementary Fig. 7) based on the DFT model agree with the experimental results in a quantitative way (Supplementary Table 1), further verifying the validity of the DFT model. The negatively charged Au substrate and bridging water molecules may mimic the electric charges on the walls of biological and artificial ion channels in stabilizing the compact K^+ structures[13,17]. Such a compact K^+–water chain structure can promote the concerted ion movement through the direct Coulomb knock-on mechanism[18,20].

Single 1D Na^+–water chains

The hydrated Na^+ can also form a 1D chain structure in the hcp regions of the Au(111) surface (Fig. 2a, upper panel). The Na^+–water chain is similar to the K^+–water chain in height but wider (Fig. 2a, lower panel). The high-resolution AFM image at a large tip height reveals that the Na^+ ions (round depressions) are surrounded by four water molecules and connected with each other through one bridging water molecule (indicated by white (black) arrows in Fig. 2b,c (d)). Meanwhile, the Na^+ are grouped every three ions, and the resulting Na^+ trimers form a periodic structure along the chain direction (Fig. 2b, left). At a smaller tip height, the H-bonding skeleton of the surrounding water molecules is resolved (Fig. 2b, right). The AFM images at different tip heights allow determination of the atomic structure of the Na^+–water chain with high accuracy (Fig. 2d, Supplementary Fig. 8 and Supplementary Table 2). The simulated AFM images (Fig. 2c) quantitatively reproduce the experimental results.

We noted that most of the water molecules in the Na^+–water chain have an H-down configuration due to the negatively charged surface (Supplementary Section 1 and Supplementary Fig. 3), except for those directly bonded with the Na^+ ions, some of which may adopt a flat-lying configuration (indicated by red arrows in Fig. 2b–d). These flat-lying water molecules play an essential role in forming pentagon structures (highlighted by dashed lines in Fig. 2b–d) and stabilizing the chain. Moreover, there are three equivalent configurations of the flat-lying water molecules, which can switch between the three (Supplementary Section 3 and Supplementary Fig. 9). The flat-lying water molecules are adsorbed higher above the surface than the H-down ones due to the weaker interaction with the surface, thus appearing as bright protrusions in the AFM images (Fig. 2b,c, left).

The structure of the Na^+–water chain is qualitatively different from that of the K^+–water chain. First, the Na^+ ions in the trimer structure are bridged by only one water molecule, while the K^+ ions have two bridging water molecules, indicating that the hydration shell of Na^+ is more crowded than that of K^+. Second, only three Na^+ ions can be brought close to contact, while in the K^+ case up to 22 ions form a closely contacted chain in our experiments. Third, the Na^+–water chain has a higher water–ion ratio (6:1) than the K^+–water chain (3:1). These differences can be attributed to the larger dehydration energy and charge density of Na^+ than K^+ (Supplementary Table 3), making it more difficult to remove water molecules from the hydration shells to form a close ionic contact structure. We also report the chain structure of Li^+, which has even larger dehydration energy than Na^+. Indeed, direct ion–ion contact is absent from the Li^+–water chain, and the water–ion ratio (18:1) is much larger than that of the Na^+–water chain (Supplementary Section 4 and Supplementary Fig. 10). It is interesting to observe that the ion–water ratio and the degree of close ion packing follow the sequence $K^+ > Na^+ > Li^+$ (Supplementary Fig. 11), resembling the permeation and selectivity sequence of biological and artificial potassium channels[11,14,17,30].

Driving force for the close ionic packing

To explore the driving force for the close nanoscale packing of alkali ions at interfaces, we performed controlled tip manipulation experiments on the K^+–water chain (Fig. 3 and Methods). As shown in Fig. 3a by the red arrow, we used the tip to drag one short K^+–water chain to approach another in an end-to-end way. At first, the two water molecules at the end of the K^+–water chain interlink the two chains (Fig. 3b). Next, under the relaxation processes (Methods), the right-end water

https://doi.org/10.1038/s41565-023-01550-9

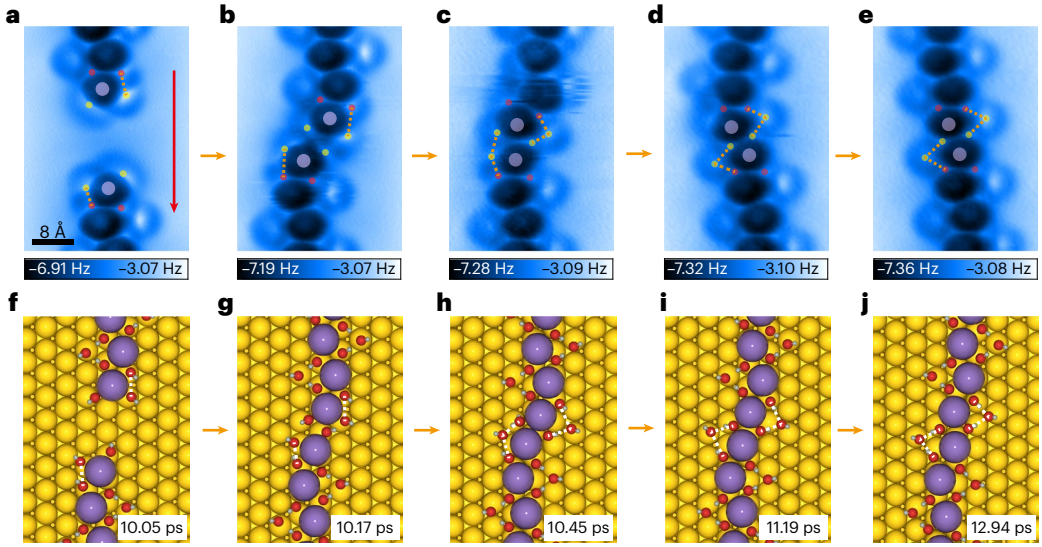

Fig. 3 | Formation process of the 1D K^+–water chain. a–e, Constant-height AFM images of two separate (**a**), metastable (**b–d**) and stable (**e**) structures of 1D K^+–water chains. Two separate K^+–water chains were manipulated by the tip to approach each other (see the red arrow). For details of the tip manipulation, see Methods. In all AFM images, the yellow and red balls highlight the end and bridging water molecules, respectively. Tip heights of the AFM images: 50 pm, referenced to the STM set point on the Au substrate (50 mV, 30 pA). All the experiments were performed at 5 K. **f–j**, MD snapshots showing the aggregation of two separate 1D K^+–water chains at 50 K. To simulate the tip manipulation, an initial equivalent kinetic energy was assigned to the two short K^+–water chains, making them move towards collision. The dashed lines represent the H bonds between the water molecules.

molecule of the upper chain was detached from the K^+ and it formed an H bond with the right-end water molecule of the lower chain, which then became a bridging water molecule to connect the two chains (Fig. 3c). The same process happened on the left side (Fig. 3d), finally resulting in a complete longer K^+–water chain (Fig. 3e). Once the zig-zag structure formed, applying further voltage pulses was unable to disturb the structure, indicating its high stability. Such a sequence of chain formation through partial ion dehydration is nicely reproduced by molecular dynamics (MD) simulation (Fig. 3f–j, Methods, Supplementary Section 5, Supplementary Fig. 12 and Supplementary Video 2). Via DFT calculations, we demonstrate that a longer K^+–water chain (six K^+ ions) is energetically more favourable than two shorter chains (three K^+ ions) by ~420 meV.

From the manipulation experiments and MD simulations, it is clear that the water molecules in the hydration shell of K^+ are inclined to detach from the ion and form new H bonds with other water molecules. Such a tendency can be understood by considering that the water–K^+ interaction is weaker than the water–water interaction[31]. These water–water H bonds then drag the two K^+–water chains to approach each other through the water–ion interaction, finally leading to the close contact of K^+ ions. Therefore, it is the interplay between the water–ion and water–water interactions that yields an effective attraction between the ions. To quantitatively compare the contributions of different interactions during the chain interconnection, we carried out crystal orbital Hamilton population and integrated-crystal orbital Hamilton population analysis based on the LOBSTER calculations (Supplementary Section 6, Supplementary Figs. 13 and 14). These results suggest that the energy gain related to the water–water H-bonding interaction (−1,038 meV) is much larger than that of K^+–water interaction (−70 meV), K^+–Au substrate interaction (+50 meV) and dipole–dipole interaction between water molecules (−167 meV, Supplementary Section 7). Therefore, the water–water interaction constitutes the major contribution to overcoming the K^+–K^+ Coulomb repulsion (+806 meV), promoting the formation of K^+–water chains (Supplementary Section 8 and Supplementary Fig. 15). The tendency for the ions to become closely packed is inversely correlated with the strength of ion–water interaction. Such a phenomenon is analogous to the spontaneous aggregation of hydrophobes in water through hydrophobic interaction[32,33]. However, if the ion–water interaction is too weak, it is difficult to maintain the water H-bonding network around the ion chain, and the closely packed ion chain may not be stable. Indeed, we failed to obtain a 1D Cs^+–water chain structure on Au(111) due to the relatively weak Cs^+–water interaction (Supplementary Fig. 11).

It is unexpected that the hydrated alkali ions can spontaneously polymerize into 1D chains on the atomically flat surface, where the confinement is much less severe than that of the 1D ion channel. We notice that each alkali ion (Li^+, Na^+ and K^+) is always coordinated by four water molecules in the 1D chain at the Au(111) surface. In contrast, the H-bonding interaction between the water molecules prefers the hexagonal structure[23,26,28]. There is a symmetry mismatch between the hydrated ions and the H-bonding structure of water, leading to five-, four- and even three-membered water rings in the ion–water chains with a substantial increase in strain energy. Compared with the 2D structure, the formation of the 1D chain structure can give more freedom to release the strain energy and optimize the H-bonding interaction.

1D K^+–water chains embedded within the 2D water network

To investigate the robustness of 1D ion chains, we performed further experiments on K^+ systems at higher water–ion ratios. At a particular water–ion ratio of 4:1, the hydrated K^+ can self-assemble into a 2D network through the water molecules (Fig. 4a–d). However, the H bonds between the water molecules are distorted due to the tetragonal symmetry of the hydrated K^+. Such a structure is fragile and can be easily converted to a more stable chain structure under tip disturbance (Supplementary Fig. 16) or an increase of the water–cation ratio (Fig. 4e–i). At a higher water–ion ratio (~6:1), some of the K^+ ions dehydrate and locally aggregate (Fig. 4e–h), resulting in a closely packed chain structure similar to that shown in Fig. 1. Such a structure change could be understood through the DFT analysis of thermodynamic stability of the different water–ion structures in terms of the K chemical potential, which shows that the 2D network with the water–ion ratio of 4:1 is energetically favourable only within a narrow range of

https://doi.org/10.1038/s41565-023-01550-9

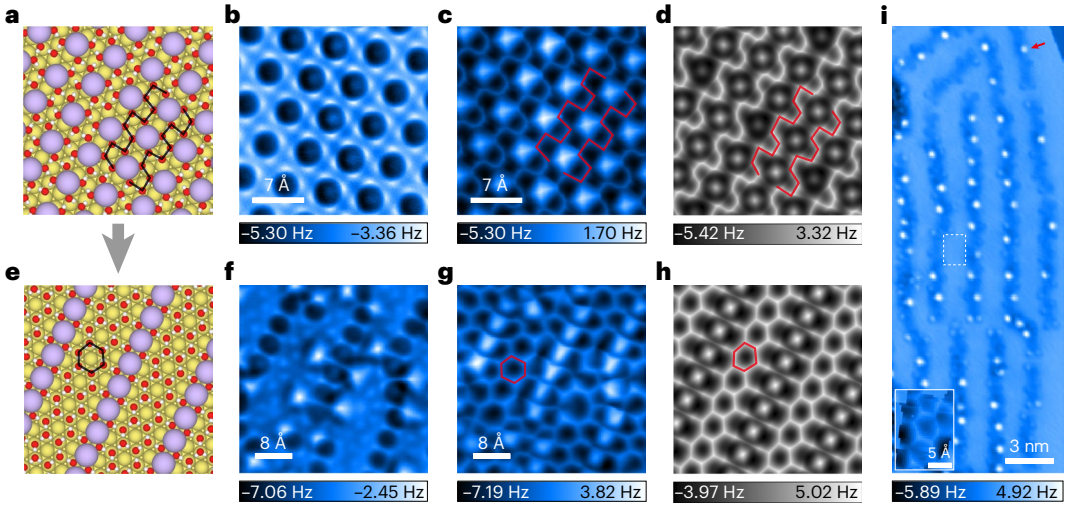

Fig. 4 | 2D K^+–water networks at different water-to-ion ratios. a–d, Structural model (**a**), AFM (**b**,**c**) and simulated AFM (**d**) images of the 2D K^+–water network at a water–ion ratio of 4:1. **e–h**, Structural model (**e**), AFM (**f**,**g**) and simulated AFM (**h**) images of the 2D K^+–water network at a higher water–ion ratio, showing the local 1D aggregation of K^+. **i**, AFM image of the periodic K^+ array structure formed by further increasing water–ion ratio, which is embedded in the 2D water network. A water molecule adsorbed on top of K^+ is indicated by the red arrow. The hexagonal H-bonding network of water between the K^+–water chains is shown in the inset. The black (red) lines in **a** and **e** (**c**, **d**, **g** and **h**) highlight the H bonds between the water molecules in the structural model (experimental and simulated AFM images). The tip heights of **b**, **c**, **f**, **g** and **i** are 50 pm, −30 pm, 50 pm, −50 pm and 350 pm, respectively, referenced to the STM set point on the Au substrate (100 mV, 10 pA). The tip heights of **d** and **h** are 11.00 Å, defined as the vertical distance between the apex atom of the metal tip and the outermost atom of the Au substrate. The oscillation amplitude of experimental and simulated images is 100 pm. Au, K, H and O atoms are denoted by yellow, purple, white and red spheres, respectively, in structural mode. All the experiments were performed at 5 K.

K chemical potential and could transform to the chain structures with a water–ion ratio of 3:1 or 6:1 (Supplementary Section 9 and Supplementary Fig. 17).

When the water–ion ratio further increases, additional water molecules will adsorb on top of the K^+–water chain, providing a three-dimensional screening environment and stabilizing the K^+–water chain. In such a case, the K^+–water chains can even form periodic arrays, which are precisely aligned and embedded in the 2D hexagonal water network (Fig. 4i and Supplementary Fig. 18). The orientation of K^+–water chains has no registry with the atomic arrangement of the Au(111) substrate (Supplementary Fig. 19), which reveals that the surface lattice plays a negligible role in forming a 1D ion chain. In addition, we report that the 1D K^+–water array can remain stable at temperatures up to 135 K before water desorption occurs. For practical 1D or 2D ion channels under physiological/ambient conditions, the water and ions are strictly confined, and desorption is unlikely to occur[2,5,6,13]. Therefore, over a wide range of water–ion ratios and temperatures, the ions can aggregate into a 1D structure to preserve the hexagonal H-bonding network of water, such that both the water–ion and water–water interactions are optimized.

Robustness of the 1D ionic chains and perspective

In addition to the Au(111) surface, we found that similar 1D ion chains are also present on the single-crystal Pt(111) and monolayer graphene/Cu(111) surfaces. The Pt(111) surface is more hydrophilic than the Au(111) surface and facilitates the formation of water monolayer structure, thus alkali ions could be incorporated into the hexagonal H-bonding network of water at low concentration (~1.5 M), locally forming 1D chain structures (Supplementary Section 10 and Supplementary Fig. 20). Since the graphene/Cu(111) surface is more hydrophobic than the Au(111) surface and provides less ionic screening, the ions and water molecules can construct periodic arrays embedded in the 2D water network as in Fig. 4i (Supplementary Section 11 and Supplementary Fig. 21), where the top absorbed water molecules could enhance the screening effect and assist in formation of the ion chain. The lack of responsiveness to stimuli of the ionic chains to the various surfaces and the water–ion ratio suggests that the 1D polymerization of alkali ions might be considered a general response for different confined geometries.

To investigate our findings in practical nanofluidic systems at ambient conditions, we carried out MD simulations containing K^+ cations and water molecules on the Au surface and in a structural 2D graphitic nanochannel with a height of ~6 Å (internal space of ~3 Å) at different temperatures (Supplementary Videos 3–5). We found that similar close-packing ion chain structures also exist under strong 2D confinement, and the lifetime (up to 150 ps) is almost one order of magnitude longer than that on the Au surface (half confinement) at 300 K (up to 15 ps). We suggest that the stability of a close-packing structure is governed by both kinetic and thermodynamic factors and could be further enhanced under 2D/1D confinement (Supplementary Section 12). Given that the ion diffusion through the ion channels typically occurs on a timescale of several picoseconds to tens of nanoseconds at ambient temperature (~300 K), these densely packed ion chain structures are expected to promote concerted and directional ion movement through Coulomb interactions. This feature paves the way for understanding fast ion transport in 1D and 2D nanoscale channels with charged interfaces[4,17]. Additionally, the presence of anions in the 2D monolayer graphene nanochannel could further enhance the stability of 1D cation chains[19].

The specific hydration structure of the ion chains could lay new foundations for comprehending the ion selectivity of ion channels and offer an improved perspective on understanding the high permeation efficiency of the K^+ channel (Supplementary Fig. 11). The hydration energy of the K^+ ion lies in a middle position among different alkali metal cations, competing with water–water interaction, which not only facilitates the ionic close packing but also maintains a sufficient H-bonding network to stabilize the chain structure (Supplementary Fig. 11). Furthermore, our results may provide general design principles for artificial ion channels towards highly efficient and precisely selective ion permeation.

Online content

Any methods, additional references, Nature Portfolio reporting summaries, source data, extended data, supplementary information, acknowledgements, peer review information; details of author contributions and competing interests; and statements of data and code availability are available at https://doi.org/10.1038/s41565-023-01550-9.

References

1. Hummer, G., Rasaiah, J. C. & Noworyta, J. P. Water conduction through the hydrophobic channel of a carbon nanotube. *Nature* **414**, 188–190 (2001).
2. Tunuguntla, R. H. et al. Enhanced water permeability and tunable ion selectivity in subnanometer carbon nanotube porins. *Science* **357**, 792–796 (2017).
3. Garaj, S. et al. Graphene as a subnanometre trans-electrode membrane. *Nature* **467**, 190–193 (2010).
4. Joshi, R. K. et al. Precise and ultrafast molecular sieving through graphene oxide membranes. *Science* **343**, 752–754 (2014).
5. Shen, J., Liu, G. P., Han, Y. & Jin, W. Q. Artificial channels for confined mass transport at the sub-nanometre scale. *Nat. Rev. Mater.* **6**, 294–312 (2021).
6. Radha, B. et al. Molecular transport through capillaries made with atomic-scale precision. *Nature* **538**, 222–225 (2016).
7. Suo, L. M. et al. 'Water-in-salt' electrolyte enables high-voltage aqueous lithium-ion chemistries. *Science* **350**, 938–943 (2015).
8. Chao, D. L. et al. Roadmap for advanced aqueous batteries: from design of materials to applications. *Sci. Adv.* **6**, eaba4098 (2020).
9. Liu, T. C. et al. In situ quantification of interphasial chemistry in Li-ion battery. *Nat. Nanotechnol.* **14**, 50–56 (2019).
10. Cheng, X. B., Zhang, R., Zhao, C. Z. & Zhang, Q. Toward safe lithium metal anode in rechargeable batteries: a review. *Chem. Rev.* **117**, 10403–10473 (2017).
11. Doyle, D. A. et al. The structure of the potassium channel: molecular basis of K^+ conduction and selectivity. *Science* **280**, 69–77 (1998).
12. Payandeh, J., Scheuer, T., Zheng, N. & Catterall, W. A. The crystal structure of a voltage-gated sodium channel. *Nature* **475**, 353–358 (2011).
13. Zhou, Y. F., Morais-Cabral, J. H., Kaufman, A. & MacKinnon, R. Chemistry of ion coordination and hydration revealed by a K^+ channel–Fab complex at 2.0 Å resolution. *Nature* **414**, 43–48 (2001).
14. Chen, L. et al. Ion sieving in graphene oxide membranes via cationic control of interlayer spacing. *Nature* **550**, 415–418 (2017).
15. Schoch, R. B., Han, J. Y. & Renaud, P. Transport phenomena in nanofluidics. *Rev. Mod. Phys.* **80**, 839–883 (2008).
16. Zhu, Z. P., Wang, D. Y., Tian, Y. & Jiang, L. Ion/molecule transportation in nanopores and nanochannels: from critical principles to diverse functions. *J. Am. Chem. Soc.* **141**, 8658–8669 (2019).
17. Xue, Y. et al. Atomic-scale ion transistor with ultrahigh diffusivity. *Science* **372**, 501–503 (2021).
18. Kopfer, D. A. et al. Ion permeation in K^+ channels occurs by direct Coulomb knock-on. *Science* **346**, 352–355 (2014).
19. Robin, P., Kavokine, N. & Bocquet, L. Modeling of emergent memory and voltage spiking in ionic transport through angstrom-scale slits. *Science* **373**, 687–691 (2021).
20. Kopec, W. et al. Direct knock-on of desolvated ions governs strict ion selectivity in K^+ channels. *Nat. Chem.* **10**, 813–820 (2018).
21. Zheng, J. X. et al. Understanding thermodynamic and kinetic contributions in expanding the stability window of aqueous electrolytes. *Chem* **4**, 2872–2882 (2018).
22. Giessibl, F. J. The qPlus sensor, a powerful core for the atomic force microscope. *Rev. Sci. Instrum.* **90**, 011101 (2019).
23. Carrasco, J., Hodgson, A. & Michaelides, A. A molecular perspective of water at metal interfaces. *Nat. Mater.* **11**, 667–674 (2012).
24. Gross, L., Mohn, F., Moll, N., Liljeroth, P. & Meyer, G. The chemical structure of a molecule resolved by atomic force microscopy. *Science* **325**, 1110–1114 (2009).
25. Peng, J. B. et al. The effect of hydration number on the interfacial transport of sodium ions. *Nature* **557**, 701–705 (2018).
26. Tian, Y. et al. Visualizing Eigen/Zundel cations and their interconversion in monolayer water on metal surfaces. *Science* **377**, 315–319 (2022).
27. Peng, J. B. et al. Weakly perturbative imaging of interfacial water with submolecular resolution by atomic force microscopy. *Nat. Commun.* **9**, 122 (2018).
28. Ma, R. Z. et al. Atomic imaging of the edge structure and growth of a two-dimensional hexagonal ice. *Nature* **577**, 60–63 (2020).
29. Shiotari, A. & Sugimoto, Y. Ultrahigh-resolution imaging of water networks by atomic force microscopy. *Nat. Commun.* **8**, 14313 (2017).
30. Mita, K. et al. Conductance selectivity of Na^+ across the K^+ channel via Na^+ trapped in a tortuous trajectory. *Proc. Natl Acad. Sci. USA* **118**, e2017168118 (2021).
31. Hribar, B., Southall, N. T., Vlachy, V. & Dill, K. A. How ions affect the structure of water. *J. Am. Chem. Soc.* **124**, 12302–12311 (2002).
32. Chandler, D. Interfaces and the driving force of hydrophobic assembly. *Nature* **437**, 640–647 (2005).
33. Meyer, E. E., Rosenberg, K. J. & Israelachvili, J. Recent progress in understanding hydrophobic interactions. *Proc. Natl Acad. Sci. USA* **103**, 15739–15746 (2006).

Methods

Sample preparation

The Au(111), Pt(111) and Cu(111) single crystals were purchased from MaTeck (initial purity 99.999% for Au(111) and Cu(111), 99.99% for Pt(111); thickness ~1 mm). The Au(111) surface was cleaned by repeated Ar^+ ion sputtering at 1 keV and annealing at about 700 K for five to eight cycles. The Pt(111) surface was cleaned by Ar^+ ion sputtering at 1 keV and annealing to 1,300–1,400 K, followed by heating at 1,000 K under an oxygen pressure of 1×10^{-7} mbar for 10–20 min to remove carbon impurities. The residual oxygen at the surface was removed by a flash annealing at 1,300–1,400 K. The Cu(111) single crystal was placed on a quartz substrate and loaded into the chemical vapour deposition furnace (Tianjin Kaiheng, custom designed with a heating area of length 20 cm and diameter 5 cm). After heating to 1,340 K under a reducing atmosphere with 500 standard cubic centimetres per minute (sccm) Ar and 10 sccm H_2, 0.01 sccm/10 sccm of CH_4/H_2 was introduced into the system for 30 min to obtain monolayer graphene. Then, the system was naturally cooled under the same reducing atmosphere. The growth was carried out under atmospheric pressure[34]. The monolayer graphene/Cu(111) surface was cleaned by annealing at about 700 K for 5 h under ~5×10^{-10} mbar. We utilized commercial alkali metal dispensers (SAES Getters), which were heated by a direct electric current to induce a chemical reaction between the chromate and the St 101 alloy, producing alkali metal atoms. The SAES alkali metal dispensers were degassed before evaporation (current I_{Li} = 8.5 A, I_{Na} = 6.7 A, I_K = 6.5 A, I_{Cs} = 5.5 A, t = 2 min). The pressure during the deposition of alkali metal atoms was maintained at a level of better than 2×10^{-9} mbar to ensure purity of the alkali metal atoms. Ultrapure H_2O (Sigma Aldrich, deuterium depleted, 1 ppm) was used and further purified under vacuum by three to five freeze-and-pump cycles to remove remaining gas impurities.

To fabricate a sample with a tunable water–ion ratio, the sample was prepared by two steps. First, the alkali metal atoms were deposited on the sample surface at temperatures ranging from 77 K to 300 K with the dosing direction along the surface normal (deposition current I_{Li} = 8.3 A, I_{Na} = 6.5 A, I_K = 6.3 A, I_{Cs} = 5.2 A, t = 1 min). Since the work functions of alkali metal (Li 2.9 eV, Na 2.36 eV, K 2.29 eV) are smaller than that of Au(111) (5.25 eV) and Pt(111) (6.10 eV), the alkali metal atoms could transfer charge to the Au(111) or Pt(111) (or monolayer graphene[35]) substrate (according to DFT calculation, Supplementary Figs. 3 and 4). The alkali metal cations could diffuse freely on the Au(111) surface even at 77 K, which exhibits a homogeneous distribution of cations across the surface (Supplementary Fig. 1a–d).

Then, the water molecules were deposited in situ onto the alkali-covered substrate surface held at 110–140 K through a dosing tube with an angle of ~40° with respect to the surface normal. For temperatures below 110 K, the thermal energy is not sufficient to obtain stable water–ion chain structures, resulting in the formation of metastable structures that are kinetically trapped. At temperatures above 140 K, the water molecules would start to desorb from the surface under the ultrahigh vacuum condition, leaving alkali metal cations alone on the surface. When the water molecules landed on the substrate, they would be frozen to 2D bilayer-ice islands and could not diffuse around the surface. This implies that the number of water molecules has a gradient across the surface (Supplementary Fig. 1e–h). By depositing alkali cations and water molecules in these two steps, we can adjust the water–ion ratio precisely through varying tip position on the same sample (Supplementary Figs. 1i–l and 20).

STM/AFM experiments

All the experiments were performed with a non-contact AFM/STM system (Createc) at 5 K using a homemade qPlus sensor equipped with a tungsten tip (spring constant $k_0 \approx 1{,}800$ N m^{-1}, resonance frequency $f_0 \approx 28.7$ kHz and quality factor $Q \approx 100{,}000$). All STM/AFM measurements were carried out at 5 K. The as-grown sample was first checked by STM at 77 K, and then quickly cooled to 5 K for further STM/AFM measurements. Throughout the experiments, bias voltage refers to the sample voltage with respect to the tip. All the STM topographic images and the AFM Δf images were obtained with the CO-terminated tips in constant-current and constant-height modes, respectively, except for those specified in the text. The CO tip was obtained by positioning the tip over a CO molecule on the Au(111) surface at a set point of 100 mV and 10 pA, followed by increasing the current to 400 pA. The oscillation amplitude of experimental AFM imaging is 100 pm.

Tip manipulation of the 1D K^+–water chain

To explore the driving force of chain formation, we tried to break and re-form the 1D K^+–water chain via controlled tip manipulation.

1. Separation of a long K^+–water chain. We applied a voltage pulse (2 V, 20 ms duration) in between two adjacent K^+ cations with the tip lift of 100 pm with respect to the STM set point of 50 mV, 30 pA. The hot electrons injected by this voltage pulse could efficiently break the long K^+–water chain into two shorter chains.
2. Displacement of a shorter K^+–water chain. We used the tip to drag one shorter K^+ chain to approach another at a small tip height with respect to the STM set point of 5 mV, 800 pA. Such tip manipulation can be efficient for the movement of short chains with a number of K^+ cations less than six.
3. Relaxation of a metastable K^+–water chain. When dragging the K^+–water chains to aggregate, the chain may stay in different metastable states, as shown in Fig. 3b–d. To facilitate the formation of more stable states, we applied a voltage pulse (300 mV, 20 ms duration) to the metastable chain at a tip height of 0 pm with respect to the STM set point of 50 mV, 30 pA. After several sequential pulses, we obtained a complete 1D zigzag K^+–water chain, as shown in Fig. 3e. Once the 1D zigzag structure formed, applying further voltage pulses was unable to disturb the structure, indicating its high stability.

DFT calculations

DFT calculations were performed using the Vienna ab initio simulation package[36,37]. Projector augmented wave pseudopotentials were used with a cutoff energy of 550 eV for the expansion of the electronic wave functions[38]. Van der Waals corrections for dispersion forces were considered by using the optB86b-vdW functional[39,40]. The surface model was constructed with an Au(111) substrate, which was modelled using a slab of more than three layers, fixed except for the top layer. The lattice constant for Au was set to be 4.073 Å. For the Li^+ model, we used a $(4 \times 6\sqrt{3})$ supercell and a $(2 \times 1 \times 1)$ Monkhorst–Pack (MP) grid for the sampling of the Brillouin zone. For the Na^+ model, we used a $(\sqrt{67} \times \sqrt{21})$ supercell and a $(1 \times 2 \times 1)$ MP grid. For the K^+ model, we used a $(3 \times 5\sqrt{3})$ supercell and a $(2 \times 2 \times 1)$ MP grid. The thickness of the vacuum slab was greater than 16 Å and the dipole correction was applied along the surface normal direction[41,42]. The detailed periodic cell dimensions for the systems can be seen in Supplementary Table 4. The geometry optimizations were performed with a force criterion of 0.01 eV Å^{-1}. The charge distribution was evaluated using the Bader charge analysis[43].

AFM simulations

The Δf images were simulated with a molecular mechanics model including the electrostatic force, on the basis of the methods described in ref. 44. We used the following parameters of the flexible probe-particle tip model: effective lateral stiffness k = 0.75 N m^{-1} and effective atomic radius R_c = 1.661 Å. For the (Li^+, Na^+, K^+) model, a quadrupole-like (d_{z^2}) charge distribution at the tip apex was used to simulate the CO tip with $q = -0.1\,e$, $-0.1\,e$, $-0.2\,e$, respectively. The input electrostatic potentials of the ion hydrates on the Au(111), employed in AFM simulations, were obtained from DFT calculations. Parameters of Lennard-Jones pairwise potentials for all elements are listed in Supplementary Table 5. The tip height in the AFM simulations is defined

as the vertical distance between the metal tip apex and the topmost layer of the substrate. The oscillation amplitudes of the simulated AFM images are 100 pm.

MD simulations

All the MD simulation results shown in the paper were obtained by using the force field parameters fitted with DFT results combined with the flexible SPC/E water model[45], ion parameters taken from ref. 46 and monolayer graphene parameters taken from ref. 19. All simulations were performed with the MD package SPONGE[47]. Two systems were constructed for the study. In the first system, K^+ ions and water molecules were arranged on a four-layer Au crystal with a (111) surface. In the second system, two bilayer graphene sheets were assembled at a distance of 6 Å, with K^+ ions and water molecules inserted between the sheets. Each simulation system was first subjected to 10,000 steps of steepest-descent energy minimization. Following this, a canonical ensemble simulation was conducted. The temperature was controlled using the middle scheme of Langevin dynamics[48] with a collision frequency of 10 ps^{-1}. The SETTLE algorithm[49] was employed to maintain the rigidity of water molecules. For the first system, the position of the bottom Au layer and the z coordinates of K^+ ions and O atoms were treated as frozen to reproduce the experimental and DFT results precisely. For the second system, all of the positions of the bilayer graphene atoms were restrained. All classical MD simulations were carried out under periodic boundary conditions. The detailed periodic cell dimensions for the systems can be seen in Supplementary Table 6. A cutoff of 7 Å was used for van der Waals interactions. We conducted tests using longer cutoffs up to 12 Å and found that the changes in simulation results were negligible. For the simulations on the Au surface, image charges were included to maintain neutrality and better describe the Au metal polarization. The finite-element Green's function method (Supplementary Section 5 and Supplementary Fig. 12) was used to calculate the electrostatic interactions. To validate the numerical correction of our method, we also used the particle mesh Ewald method[50] and found that our results are consistent with this method within floating-point precision for energy and force values (Supplementary Table 7). For the simulations of the graphene system, the carbon atoms of the graphene were equally negatively charged to maintain neutrality and the particle mesh Ewald method was used to process the electrostatic interactions.

The corresponding energy function has two terms, including a Lennard-Jones representation of dispersion–attraction and core repulsion, and a Coulombic treatment of the electrostatic interactions:

$$E = \sum_{ij} 4\varepsilon_{ij}\left[\left(\frac{\sigma_{ij}}{r_{ij}}\right)^{12} - \left(\frac{\sigma_{ij}}{r_{ij}}\right)^{6}\right] + \sum_{ij}\frac{q_i q_j}{4\pi\epsilon_0 r_{ij}}. \quad (1)$$

Here, r_{ij} is the distance between the two atoms, ε_{ij} and σ_{ij} are the parameters of the Lennard-Jones potential, q_i and q_j are the point charges of the atoms and ϵ_0 is the permittivity of vacuum. The parameters of the MD simulations are shown in Supplementary Tables 8 and 9.

Two separated K^+–water chains (each chain is made of 6 K^+ and 18 water molecules) were placed on the Au surface to simulate the formation of a single K^+–water chain (Fig. 3f–j). A 10 ps structural relaxation at 50 K was performed, then an initial equivalent kinetic energy of 347.2 meV was assigned to the two K^+–water chains to move towards collision. A 20 ps simulation at 50 K was performed, through which a single K^+–water chain was formed (Supplementary Video 2). The time step was taken as 0.1 fs.

To connect our results to realistic nanofluidic systems at ambient conditions, we performed MD simulations on two systems: 125 K^+ ions and 375 water molecules placed on an Au surface and 100 K^+ and 300 water molecules inserted between two bilayer graphene sheets. The two systems were simulated at 100 K and 300 K with a time step of 1 fs, and each simulation was performed for 1 ns (Supplementary Videos 3–5).

Data availability

Source data are provided with this paper. All other data that support the findings of this study are available from the corresponding authors upon reasonable request.

References

34. Xu, X. Z. et al. Ultrafast epitaxial growth of metre-sized single-crystal graphene on industrial Cu foil. *Sci. Bull.* **62**, 1074–1080 (2017).
35. Ohta, T., Bostwick, A., Seyller, T., Horn, K. & Rotenberg, E. Controlling the electronic structure of bilayer graphene. *Science* **313**, 951–954 (2006).
36. Kresse, G. Ab-initio molecular-dynamics for liquid-metals. *J. Non-Cryst. Solids* **193**, 222–229 (1995).
37. Kresse, G. & Furthmuller, J. Efficient iterative schemes for ab initio total-energy calculations using a plane-wave basis set. *Phys. Rev. B* **54**, 11169–11186 (1996).
38. Kresse, G. & Joubert, D. From ultrasoft pseudopotentials to the projector augmented-wave method. *Phys. Rev. B* **59**, 1758–1775 (1999).
39. Klimes, J., Bowler, D. R. & Michaelides, A. Chemical accuracy for the van der Waals density functional. *J. Phys. Condens. Matter* **22**, 022201 (2010).
40. Klimes, J., Bowler, D. R. & Michaelides, A. Van der Waals density functionals applied to solids. *Phys. Rev. B* **83**, 195131 (2011).
41. Neugebauer, J. & Scheffler, M. Adsorbate–substrate and adsorbate–adsorbate interactions of Na and K adlayers on Al(111). *Phys. Rev. B* **46**, 16067–16080 (1992).
42. Makov, G. & Payne, M. C. Periodic boundary-conditions in ab-initio calculations. *Phys. Rev. B* **51**, 4014–4022 (1995).
43. Henkelman, G., Arnaldsson, A. & Jonsson, H. A fast and robust algorithm for Bader decomposition of charge density. *Comput. Mater. Sci.* **36**, 354–360 (2006).
44. Hapala, P. et al. Mechanism of high-resolution STM/AFM imaging with functionalized tips. *Phys. Rev. B* **90**, 085421 (2014).
45. Berendsen, H. J. C., Grigera, J. R. & Straatsma, T. P. The missing term in effective pair potentials. *J. Phys. Chem.* **91**, 6269–6271 (1987).
46. Joung, I. S. & Cheatham, T. E. Molecular dynamics simulations of the dynamic and energetic properties of alkali and halide ions using water-model-specific ion parameters. *J. Phys. Chem. B* **113**, 13279–13290 (2009).
47. Huang, Y. P. et al. SPONGE: a GPU-accelerated molecular dynamics package with enhanced sampling and AI-driven algorithms. *Chin. J. Chem.* **40**, 160–168 (2022).
48. Zhang, Z. J. et al. A unified thermostat scheme for efficient configurational sampling for classical/quantum canonical ensembles via molecular dynamics. *J. Chem. Phys.* **147**, 034109 (2017).
49. Miyamoto, S. & Kollman, P. A. SETTLE: an analytical version of the SHAKE and RATTLE algorithm for rigid water models. *J. Comput. Chem.* **13**, 952–962 (1992).
50. Essmann, U. et al. A smooth particle mesh Ewald method. *J. Chem. Phys.* **103**, 8577–8593 (1995).

Acknowledgements

We thank L. Jiang, B. Song and F. Pan for inspiring discussions and the computational resources provided by the TianHe-1A, TianHe-2 supercomputer, High-Performance Computing Platform of Peking University. This work was supported by the National Key R&D Program under grants 2021YFA1400500 and 2017YFA0205003, the National Natural Science Foundation of China under grants 11888101, U22A20260, 21725302, 11935002, 21902013 and 92053202, the Strategic Priority Research Program of Chinese Academy of

Sciences under grants XDB28000000 and XDB33000000, the China Postdoctoral Science Foundation under grants 2022M720003 and 2023T160011 and the Key R&D Program of Guangdong Province under grant 2020B010189001. Y.J. acknowledges the support by the New Cornerstone Science Foundation through the New Cornerstone Investigator Program and the XPLORER PRIZE.

Author contributions

Y.J. and E.-G.W. designed and supervised the project. Y.T. and J.H. performed the STM/AFM measurements with R.M., S.Y. and D.G. Y.S., D.C., J.C. and L.-M.X. performed ab initio DFT calculations. Y.X., Y.H. and Y.Q.G. carried out the classical MD simulations. Y.S. carried out the theoretical simulations of the AFM images. M.Z.Z. and K.H.L. prepared the monolayer graphene/Cu(111) sample. Y.T., Y.S., Y.X., J.H., Y.H., J.C., C.S., Y.Q.G., E.-G.W. and Y.J. analysed the data. Y.J., Y.T., Y.S., Y.X., L.-M.X. and Y.Q.G. wrote the paper with input from all other authors. The paper reflects the contributions of all authors.

Competing interests

The authors declare no competing interests.

Additional information

Supplementary information The online version contains supplementary material available at https://doi.org/10.1038/s41565-023-01550-9.

Correspondence and requests for materials should be addressed to Li-Mei Xu, Yi Qin Gao, En-Ge Wang or Ying Jiang.

Peer review information *Nature Nanotechnology* thanks Kai Xiao, Francois Peeters, Taesung Kim and the other, anonymous, reviewer(s) for their contribution to the peer review of this work.